PAPER

Large current-induced broadening of the superconducting transition in Mo/Au transition edge sensors

View the article online for updates and enhancements.

IOP ebooks™

Bringing you innovative digital publishing with leading voices to create your essential collection of books in STEM research.

Start exploring the collection - download the first chapter of every title for free.

Large current-induced broadening of the superconducting transition in Mo/Au transition edge sensors

Lourdes Fàbrega[1], **Agustín Camón**[2], **Carlos Pobes**[2],
Pavel Strichovanec[1,2] **and Raquel González-Arrabal**[3]

[1] Institut de Ciència de Materials de Barcelona (ICMAB-CSIC), E-08193 Bellaterra, Spain
[2] Instituto de Ciencia de Materiales de Aragón (CSIC-Universidad de Zaragoza), E-50009 Zaragoza, Spain
[3] Instituto de Fusión Nuclear Guillermo Velarde y Dpto de Ingeniería Energética, ETSII (UPM), E-28006 Madrid, Spain

E-mail: lourdes@icmab.es

CrossMark

Abstract

The $R(T, I)$ shape of the superconducting transition in transition edge sensors (TESs) is of crucial importance to determine their ultimate performance. This paper reports a study of the temperature and current dependences of the transition of Mo/Au TESs, focused on the low resistance region, where these devices preferentially operate. A large broadening of the transition is observed when increasing the applied current. An empirical analytic expression for $R(T, I)$ is found, which describes the transition of devices with different critical temperatures, from $R = 0$ up to at least 30% R_n (in some cases nearly 80% R_n). Several mechanisms for this behaviour are considered; results show that a current assisted vortex pair unbinding mechanism (Berezinskii–Kosterlitz–Thouless transition) could be the possible origin for this behaviour. Finally, the consequences of the current-induced transition broadening for TES properties and operation are outlined.

Keywords: transition edge sensors, superconducting transition, vortex motion, radiation detectors

(Some figures may appear in colour only in the online journal)

1. Introduction

Transition edge sensors (TESs), constituted by a superconducting thin film or bilayer operating at a point in the resistive transition $R(T, I)$, have been shown to display extraordinary performances. TESs are currently, and plan to be, used for a variety of instruments which require extremely high sensitivities, in space and other applications [1, 2].

The shape of the superconducting transition, as well as its temperature and electrical current dependences, drastically contribute to the performance of the TES. In fact, two very important parameters that define the TES behaviour are the logarithmic derivatives of the resistivity as a function of temperature and as a function of current, α and β respectively. These parameters influence the noise level, limiting the spectral resolution of the detectors [3–5]. Moreover, α also

contributes to determine the effective characteristic time of the sensors.

The operation point of a TES is usually settled in the lower part of the superconducting transition, typically below 20% R_n. Therefore, the knowledge of the physical origin of the appearance of resistance in TESs is key to understand their properties and to finely tune them towards their theoretical limit. However, it is difficult to assess the physical origin of the resistivity onset since the two independent parameters used to theoretically describe a superconductor (temperature and current) cannot be kept constant when biasing the TESs in the usual negative electrothermal feedback mode [1].

The transition of TESs has been mainly interpreted based on weak link effects and on the two-fluid model [2]. However, it is well known that in superconductors the region close

to the dissipation onset (lower part of the transition) can be dominated by thermal fluctuations and other non-equilibrium processes. These dissipation mechanisms are, in general, associated to the motion of magnetic vortices, i.e. cylindrical supercurrents carrying one magnetic flux quantum. Many vortex phases and vortex motion regimes have been described depending on the anisotropy, the dimensionality and the disorder, and for each of them different $R(T, I, H)$ dependences have been predicted (see for instance [6] for an extensive overview). In particular, for 2D superconductors, as TESs are thought to be, the Berezinskii–Kosterlitz–Thouless (BKT) transition is considered as the most likely mechanism responsible for the appearance of a finite resistance in the absence of an external magnetic field.

Berezinskii [7] and Kosterlitz and Thouless [8] predicted a thermodynamic instability in 2D neutral superfluids. They showed that vortex–antivortex pairs, bound at low temperatures, would dissociate at a characteristic temperature named T_{BKT}. This prediction, which constitutes the so-called BKT transition, was confirmed first on superfluid helium films and later on in many other systems, among them 2D superconductors. Indeed, Beasley *et al* [9] argued that an analogous instability and phase transition should exist in superconducting films with thickness smaller than the penetration depth, because in this case the magnetic vortices display also a logarithmic interaction with distance, which is intimately connected to the BKT transition. Therefore, in 2D superconductors, at low temperature, there would exist magnetic vortex–antivortex pairs, that at the characteristic temperature T_{BKT} would dissociate [9, 10]. Above T_{BKT}, the unbound vortices (each one of them carrying one magnetic flux quantum) will be able to move by the Lorentz force when an external electric current is applied. This vortex motion generates a resistance in the superconductor at T_{BKT}, below the mean field superconducting critical temperature, T_{co} [11].

Fingerprints of the BKT transition have been observed in many conventional and unconventional superconductors as well as in Josephson junction arrays [12–17]. Several authors have pointed out that the BKT transition could also take place in TESs [18–21]. It is important to mention that since the dissipation associated to this transition shows distinctive features, it should have clear implications for the lower part of the TES $R(T)$ transition, that is, in the α and β parameters and therefore, on TES performances in the region of interest for their operation. In fact, Fraser evaluated the possible contribution of the BKT transition to the TES noise [18].

In this paper the shape of the resistive transition of Mo/Au TESs is exhaustively studied at different electrical currents, focusing on the low resistance region, where a large decrease in the dissipation onset temperature due to the electrical current is observed. For comparison, the transition under an external magnetic field is also analysed, showing that the functional dependences $R(T, I)$ and therefore, the physical origin of the dissipation, are different with and without an external magnetic field. We find out an analytical expression that describes the $R(T, I)$ shape at low R/R_n in the absence of external magnetic field, for all analysed devices. Moreover, we observe a correlation between it and the TES's

critical temperatures. The analogy of the empirical $R(T, I)$ expression with that expected for a BKT transition, and therefore its relationship with it, is discussed. It is argued that the dissipation onset in these TESs can be due to a current enhanced vortex pair unbinding. Finally, the consequences of these results for the TES operation and optimization of their performances are evaluated.

2. Experimental

Several square TESs made of high quality Mo/Au proximity bilayers with dimensions between 50–200 μm were fabricated as reported elsewhere [22]. The bilayers were deposited at room temperature. First Mo was deposited by RF magnetron sputtering in an ultra high vacuum chamber; afterwards a 15 nm thick Au layer was deposited *in situ* by DC magnetron sputtering, in order to protect the Mo surface; finally the thickness of the Au layer was increased up to the desired value by *ex situ* e-beam deposition. Both Mo and Au layers show a columnar microstructure. The column width ranges from 20–70 nm, depending on the layer thickness.

Studied devices are bare TESs without absorbers or banks, nor any other normal metal structure on their top. Analysed samples belong to different batches. The fabrication dates span over more than one year. Sputtered Nb and Nb/Mo pads were used, both with critical temperatures close to 8.8 K. Most of the studied TESs were deposited on bulk substrates (Si covered by low stress Si_3N_4), while one of them was fabricated on a Si_3N_4 membrane. The main features of the studied devices are summarized in table 1. The TES critical temperature is controlled by changing the Au layer thickness (d_{Au}) in the Mo/Au bilayer, while keeping constant the Mo layer thickness (d_{Mo}). For these devices $d_{Mo} = 100$ nm and d_{Au} ranged between 100 and 220 nm.

Electric transport measurements were performed using the four-probe configuration in a Quantum Design Physical Property Measurement System equipped with a ^{3}He head, which limited the measurements to $T > 350$ mK. For this reason, the critical temperatures of the studied devices ranged between 465 and 642 mK. $R(T)$ measurements were carried out at different, constant currents ranging from 10 to 200 μA. Currents were applied in the AC mode at low frequency (17 Hz) in order to increase sensitivity. Data were recorded always warming up and stabilizing the temperature before measuring each point. For the characterization of $R(T)$ in the presence of an external magnetic field (H), the field was applied in the direction perpendicular to the TES plane using a superconducting magnet. When measuring at $\mu_o H = 0$ mT, the remanent field was cancelled using a magnet demagnetizing sequence. I–V curves were measured at $\mu_o H = 0$ mT, under DC bias, increasing the absolute value of the current for both positive and negative current, at constant temperature and carefully watching to avoid the heating of the sample, which was at most 1 mK.

Table 1. Brief overview of the most important parameters of the devices analysed in this work. All of them are square.

T_{co} (mK)	Pads and wiring	Design	Lateral size (μm)	R_n (mΩ)	Maximum R/R_n for fits to equation (4)
642	Nb	Membrane, no banks	200	70	$\sim$30%
612	Mo/Nb	Bulk, no banks	200	70	$\sim$35%
584	Mo/Nb	Bulk, no banks	120	57	$\sim$79%
473	Mo/Nb	Bulk, no banks	120	26	$\sim$70%
467	Mo/Nb	Bulk, no banks	50	26	$\sim$70%

3. Results and discussion

3.1. Resistive transition: effects of an external electrical current and of an external magnetic field

Figure 1(a) shows the resistive transition of a TES recorded at zero magnetic field and different currents. The transition width increases with rising current, as a result of a decrease in the temperature delimiting the appearance of a finite resistance (lower end of the transition). On the contrary, the upper limit of the transition (initial resistance drop) remains nearly unchanged—within the temperature sensitivity—except for the largest applied current[4]. These results indicate that resistance depends on current all through the transition, up to values very close to the normal state resistance (R_n). The logarithmic scale in the inset highlights the huge broadening of the transition upon increasing the electrical current, taking place specially below 30% R_n. This nonlinear behaviour (i.e. resistance dependent on current) together with the large transition broadening is observed in all the devices characterized in this study.

In order to account for the possible influence of the presence of an external magnetic field on the behaviour of the transition, the $R(T)$ curves were measured under an applied field of 2 mT, at different external currents. Data for the same TES are shown in figure 1(b). By comparing figures 1(a) and (b), one can conclude that the transition behaviour measured with and without an applied external magnetic field is different, which indicates that the presence of an external magnetic field notably influences the transition shape. First, the upper limit of the transition shifts down when an external field is applied. Second, the transition broadening is much larger when a magnetic field is applied than when it is not. This fact is more clearly illustrated in figure 1(c) which shows the dependence of the shape of the transition on the external magnetic field for the same device biased at 50 μA. Here, we clearly observe that the higher the applied magnetic field, the larger the transition broadening. Note that the transition broadening at zero field and 50 μA, which is significant, as shown in figure 1(a), is not appreciated in figure 1(c) because of the selected temperature scale. Third, the transition shape itself measured without and with an external magnetic field is also notably different. If no external field is applied, the transition shows two regimes, identified as *regime I* and *regime II* in the graph (see inset in figure 1(a)), corresponding

to the points below and above the inflection displayed approximately at 30%R_n, respectively. Whereas the $R(T)$ curves measured in the presence of an external magnetic field exhibit three regimes identified as *regime I*, *regime II* and *regime III* in the graph (see inset in figure 1(b)). In this case *regime I* corresponds to the lower part of the transition curve, very steep and highly nonlinear. In *regime II*, at intermediate resistances (roughly between 10% and 30% R_n), the resistance appears linear (not dependent on current); and in *regime III*, closer to R_n, the resistance exhibits again a nonlinear behaviour.

Figure 2 shows the two characteristic temperatures delimiting the transition: the upper limit or resistance drop onset (taken[5] as 95% R_n, T_{95}), and the lower limit or dissipation onset (defined as the lowest temperature with finite resistance, T_0). This graph illustrates again the effect of the application of an external magnetic field and of the external electrical current on the transition broadening. Moreover, it can be observed that the influence in T_{95} and T_0 characteristic temperatures of an external magnetic field is different from that of an electrical current. Indeed, while T_{95} remains nearly unchanged when rising the external electrical current, it shifts to much lower temperatures when applying an external magnetic field. This shift depends on the magnitude of the field, increasing when rising it. On the other side, T_0 significantly decreases (leading to an increase in the transition width) when increasing current and magnetic field, being the magnetic field effect much larger than that of current. From these data we conclude that both the application of an external magnetic field or of an external electrical current notably influence the shape and the width of the transition temperature curve. But they do in a different way. We also observe that both effects somehow overlap.

Next, we will focus on the data measured in the absence of an external magnetic field (that is, $\mu_o H \approx 0$), since this is the regime of special interest for TES operation.

3.2. The lower resistance regime at $\mu_o H = 0$: analysis of the dissipation onset

As stated above and as seen in figure 1(a), two regimes can be clearly identified in the $R(T)$ curves at zero field, roughly corresponding to below and above 30% R_n. This behaviour is

---

[4] A shift of $\sim$2 mK in the resistance drop onset due to a current of 200 μA is fully compatible with an expected depairing current of several tens of mA.

[5] The resistance drop close to R_n is very sharp, especially at zero field. Analyses of the paraconductivity within the Aslamazov–Larkin theory have not evidenced any rounding associated to it, as expected from the low R_n. Therefore, T_{95} can be identified with the mean field critical temperature, T_{co}, within the experimental temperature uncertainty, 1 mK.
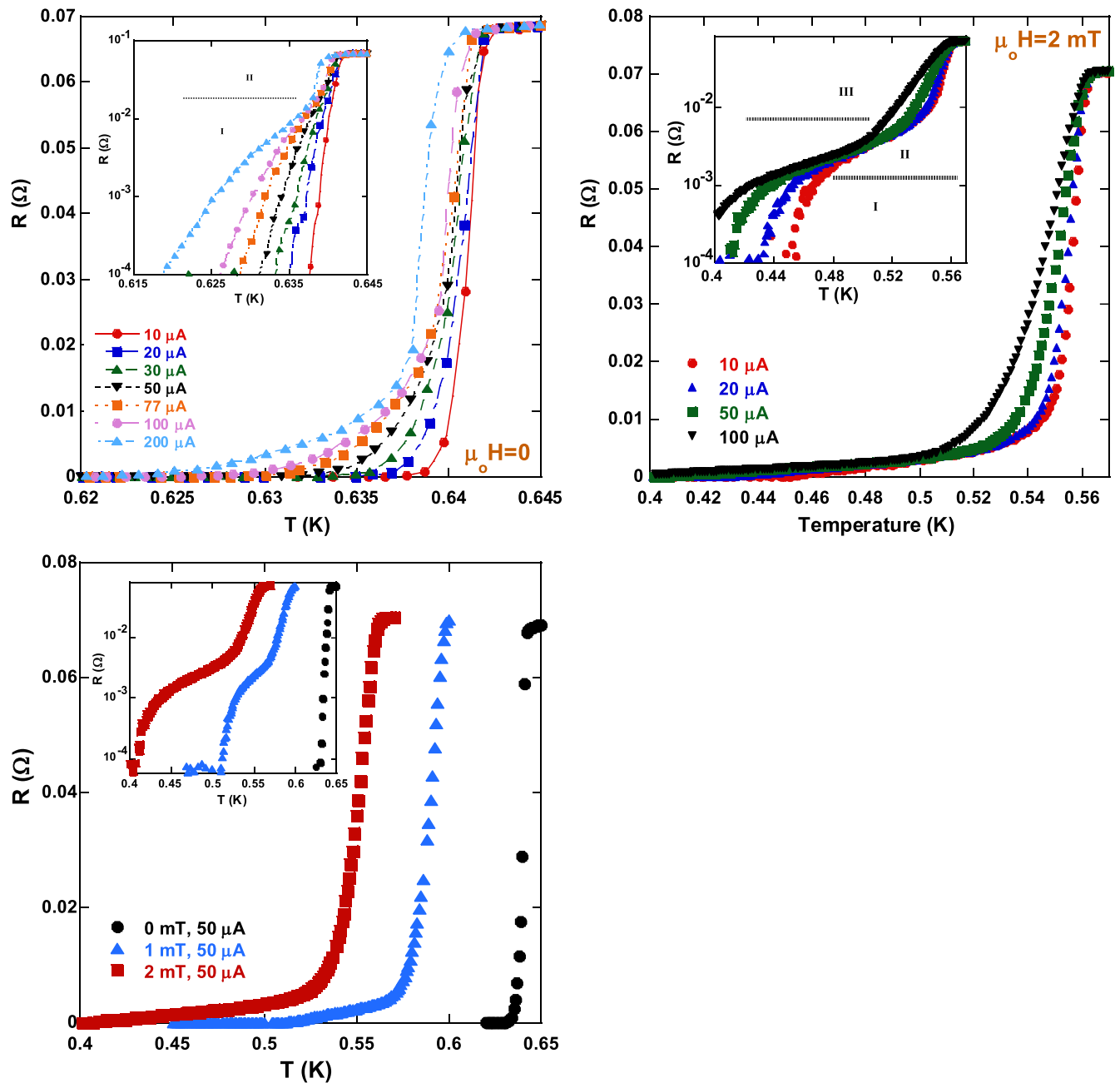
Figure 1. Resistance transition of a TES measured under different conditions: (a) zero applied external magnetic field and different applied external currents; lines are guides for the eye. (b) $\mu_o H = 2$ mT and different applied external currents. And (c) $I = 50$ μA with $\mu_o H = 0$, 1 and 2 mT. The insets in each figure (semilogarithmic scales) zoom the effects of external magnetic field and external current on the transition broadening. The horizontal lines in the insets in (a) and (b) are guides to identify the different regimes discussed in the text.

not unique for this TES but it is observed for all the measured devices although, as shown in figure 3 and in table 1, the R/R_n value delimiting the two regimes differs from 30% R_n up to 80% R_n depending on the device. No apparent correlation is found between the position of the limiting value and the TES size or critical temperature (T_{co}), for the studied devices. In order to account for such eventual dependence, more specific studies as a function of T_{co} or size should be performed with larger statistics (measuring more samples).

In the following, we will focus on the low resistance regime (*regime I* shown in figure 1(a)), because it widely covers the region of the transition most interesting for TES

operation. Nevertheless, note that the nonlinear resistance observed at higher temperatures up to nearly T_{co} (within the temperature sensitivity, 1 mK) can be neither flux flow resistance nor paraconductivity, since these must be independent of current.

In order to account for the transition behaviour observed in *regime I* (figure 1(a)), different mechanisms can be evaluated. We discard flux flow and paraconductivity, because they predict current independent $R(T)$ behaviour. In particular, we consider the possibility to fit our experimental data on the basis of the the two-fluid and the resistively shunted junction models [2]. We also look for evidences of thermal activation,
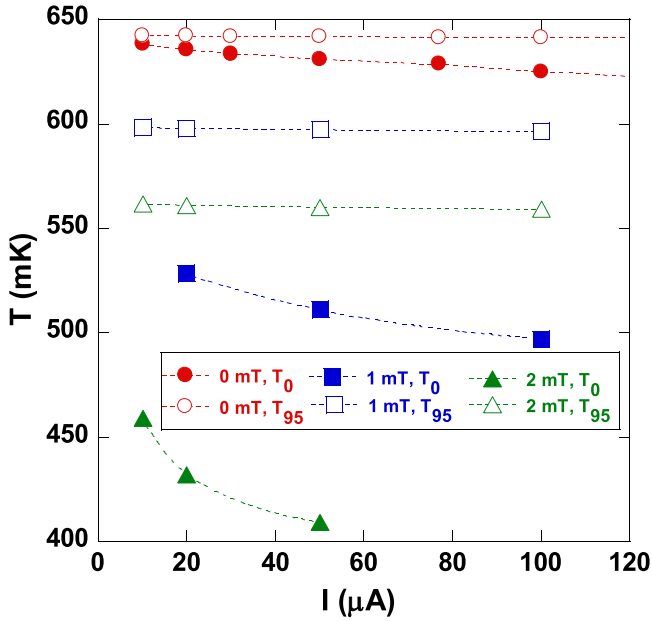
Figure 2. Characteristic temperatures delimiting the transition as a function of external electrical current, for $\mu_o H = 0$ (red dots), 1 (blue squares) and 2 mT (green triangles). The subscripts in T_{95} and T_0 state for the $\%R_n$. Thus, the vertical distance between open and full symbols of the same colour provides the transition width at each field and current. This TES has a $T_{co} = 642$ mK (see footnote 5).

since many theoretical and experimental works have evidenced the thermal activation of vortex motion as responsible of the appearance of finite resistance below the mean field critical temperature. In fact, diverse thermally activated regimes have been predicted and observed, as reviewed in [6].

The two-fluid and resistively shunted junction models propose functional dependences for $R(T, I)$ (respectively equation (17) and equations (14), (26) in [2]), significantly different from those of the data depicted in figure 3, and therefore they do not allow us to fit measured data. An Arrhenius law $\ln R \sim 1/T$, expected in general for thermally activated processes, can reasonably fit the data shown in figure 3, but only in a narrow window, corresponding to the higher resistance values of regime I; at lower resistances, closer to $R = 0$, experimental data progressively deviate from the Arrhenius law.

As stated in the introduction, a most likely mechanism for the appearance of resistance in 2D superconductors at zero applied external magnetic field is the thermally activated vortex pair unbinding [9, 10]. In view of the failure of all the other transition mechanisms considered to describe the experimental data, we take into account extensively in the following this mechanism, which will be shown to be able to describe the measured transition shape in the low resistance regime.

In 2D superconductors there are magnetic vortex–antivortex pairs. Thermal fluctuations break these vortex pairs at a characteristic temperature $T_{BKT} < T_{co}$, in what is called the BKT transition. Once this happens, free vortices can move in the presence of an external applied current because of the Lorentz force. This originates a finite resistance which

according to Kadin *et al* [23] is described by:

$$\ln\left[\frac{R(T)}{R_n}\right] \sim -2b\left[\frac{T_{co} - T}{T - T_{BKT}}\right]^{1/2}, \quad (1)$$

where b is a constant factor of the order of unity, and T_{BKT} is defined by the following relationship:

$$\frac{T_{co} - T_{BKT}}{T_{co}} \approx \frac{0.17R_n}{R_c}\varepsilon \quad (2)$$

being $R_c = 4100\ \Omega$ and ε a factor close to the unity. On these bases, equation (2) predicts a T_{BKT} whose value is very close to T_{co}. This makes T_{BKT} difficult to be observed, except for dirty (very resistive) superconductors. However, the BKT transition has not been only observed for dirty superconductors, as predicted, but also for quite clean superconductors [14] and also in superconductors with inhomogeneities [17]. In some cases, the reported T_{BKT} values are somehow lower than those calculated using equation (2).

As argued in [11, 15, 23], at temperatures lower than T_{BKT} the unbinding of vortex pairs and the consequent movement of unbound (free) vortices can be promoted by an electrical current. This implies that the resistance of a 2D superconductor is strictly equal to zero only in the absence of an external electrical current ($J = 0$). The resistance related to the free vortex motion below T_{BKT} has been predicted [6, 23] to be:

$$R \sim \left(\frac{J}{J_o}\right)^{a(T)}, \quad (3)$$

where $a(T) \sim \frac{1}{T}$ and J_o is a characteristic current of the order of the depairing critical current.

Note that the resistance at temperatures higher than T_{BKT} given by equation (1) is independent of the current, while at temperatures $T < T_{BKT}$ equation (3) describes a resistance strongly dependent on current, which follows a power law with a temperature dependent exponent. In the limit of very small currents the characteristic exponent of the power law describing the V–I curves, $V \sim I^n$, is expected to jump at $T = T_{BKT}$ from a value $n > 3$ for $T < T_{BKT}$ to $n = 1$ at higher temperatures. This jump has been traditionally considered as an experimental fingerprint of the occurrence of the BKT transition. Nevertheless, some authors have argued [15, 23] that at finite currents the BKT transition is expected to smear out, and most of its features could vanish so that its manifestation may be quite inaccessible from the experimental point of view or even unobservable. This can be even more so in the presence of flux pinning centers [14] or strong disorder, which is analysed in several recent theoretical works [24–26].

It turns out that the measured nonlinear regime observed at $\mu_o H = 0$ in the low resistance region, for all the studied TES is remarkably well described by the following equation:

$$\ln\left[\frac{R(T)}{R_n}\right] \sim -b'\left[\frac{T_{co} - T}{T - T'(I)}\right]^{1/2}. \quad (4)$$
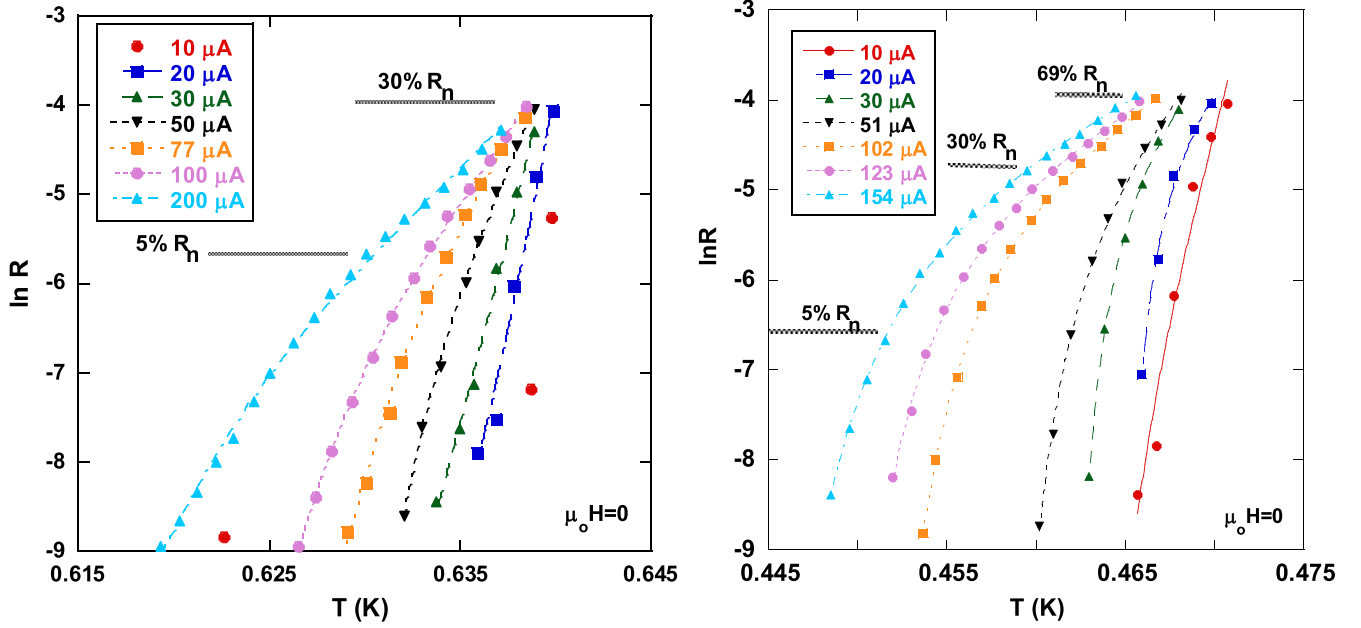
Figure 3. Lower part of the resistive transition measured at zero external magnetic field and at different external electrical currents for two different TESs with critical temperatures of 642 mK (a) and of 473 mK (b). The lines correspond to the results of the data fits to equation (4). Labeled % R_n levels evidence that fits work very well up to 30% R_n and 69% R_n, respectively.
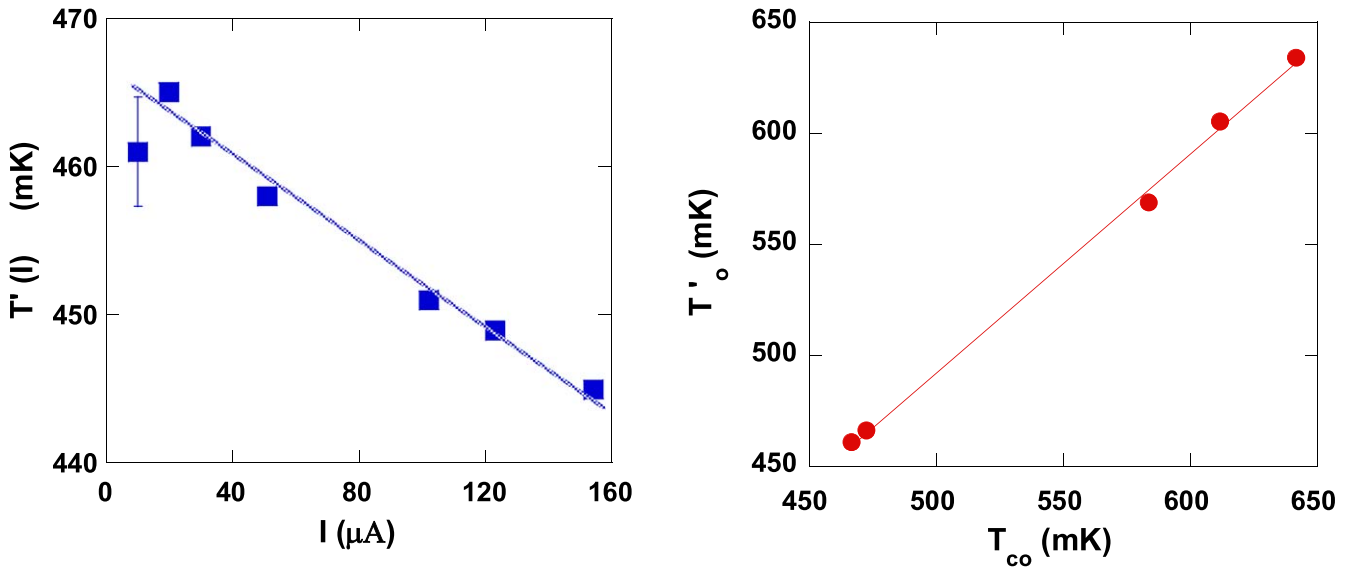

Figure 4. (a) Current dependence of the characteristic temperatures obtained from the fits performed using equation (4), for a TES with $T_{co} = 473$ mK (figure 3(b)). (b) Characteristic temperatures at zero current $T_o{}'$ defined by equation (5), for all the studied TESs, as a function of their mean field critical temperatures, T_{co}. Solid lines in both graphs are linear fits, as described in the text.

Equation (4) is formally analogue to equation (1), but with a current dependent characteristic temperature $T'(I)$ replacing T_{BKT}. For clarity, figure 3 shows the fits of the data corresponding to only two different TESs with diverse T_{co} values. The fits shown in these figures have outstanding quality, are highly reproducible, and hold for all the studied devices, always up to the kink delimiting the change of the R (T) curve (inset in figure 1(a)). It is worthwhile to mention that for the fits, the lowest current (10 μA) was usually not considered since, due to the narrowness of the transition, only very few data points are available.

The characteristic temperatures $T'(I)$ obtained from the fits to equation (4) linearly depend on the electrical current, as shown in figure 4(a). Such a linear dependence can be fitted by the following equation:

$$T' = T'_o(1 - I/I_o). \qquad (5)$$

This linear fit allows to estimate the characteristic temperature at zero electrical current (T'_o) for each particular TES. T'_o values obtained in this way are depicted in figure 4(b) as a function of the critical temperature (T_{co}). Here, it is
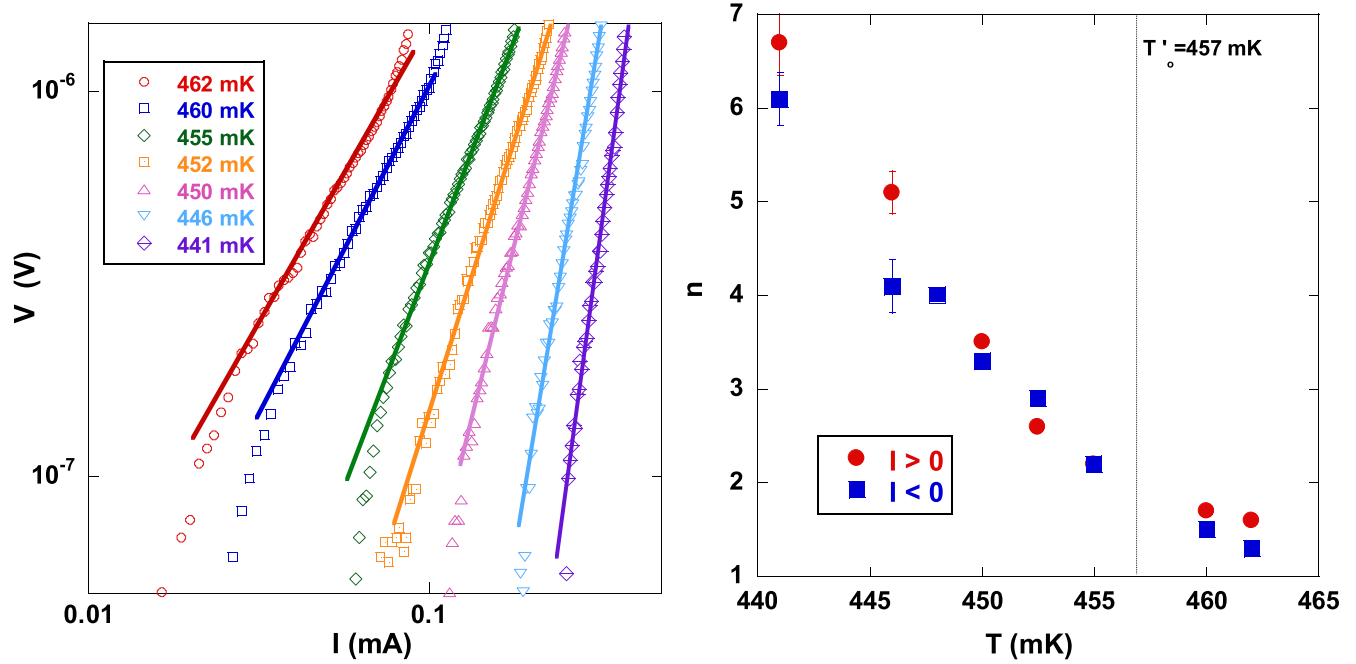
Figure 5. (a) *I–V* curves measured at zero field for a TES with $T_{co} = 467$ mK and $R_n = 28$ mΩ, at selected temperatures. The solid lines are the power law fits. (b) Exponents of the power law fits, for the positive and negative current branches of the *I–V* curves. For this TES, $T_o' = 457$ mK (vertical line).

observed that T_o' is remarkably proportional to the critical temperature ($T_o' \approx 0.98 \, T_{co}$). The values of the characteristic current I_o range from 2 up to 5 mA. No clear dependence of this characteristic current values on T_{co} is observed. Note that these I_o values are somewhat lower than the critical current values, as it will be discussed in the next section.

The similarity between the equation proposed to describe the finite resistance on the frame of the BKT transition (equation (1)) and the one that better fits our experimental data (equation (4)) strongly suggests that the observed resistance in the studied TES can be caused by a BKT transition. Until now, we have only discussed the goodness of equation (4) to fit the data measured in the absence of an external magnetic field. We have also tried to use this equation to fit the data measured in the presence of an external magnetic field (not shown). The conclusion from this trial is that equation (4) does not fit any region of the resistive transition when it is recorded in the presence of an external magnetic field, which indicates that the dissipation measured under an applied magnetic field has a different origin. Since the BKT transition should be observable only at zero magnetic field, these results provide further support to the interpretation or equation (4) in terms of the BKT transition. In the framework of a vortex pair unbinding dissipation mechanism, T_o' should be identified as the BKT temperature (T_{BKT}) while according to equation (5) $T'(I)$ could be interpreted as an effective reduction of T_{BKT} because of the enhancement of vortex pair unbinding caused by the electrical current. We note also that the electrical currents used in the analysed data are always below 10% of the characteristic currents I_o, implying that even though their effect is evident they can be considered as low; this suggests that the linear $T'(I)$

relationship given by equation (5) could only be valid at low enough currents.
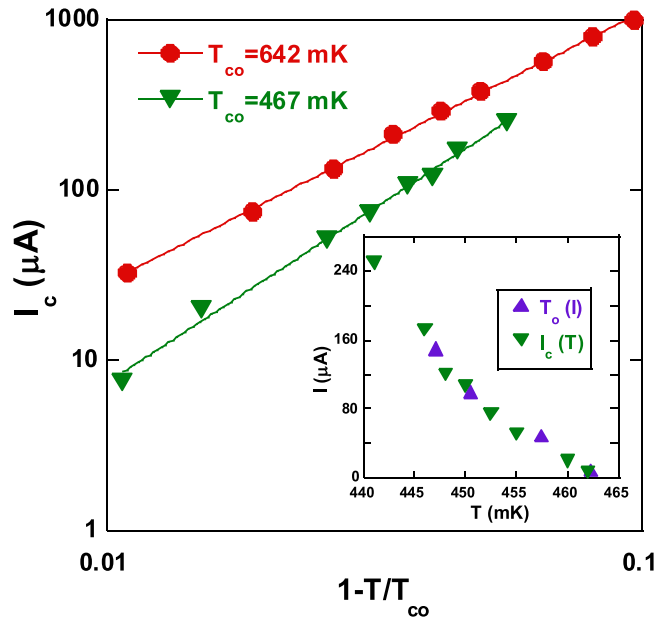
3.3. I–V curves and critical currents

Up to now, we have shown that the only formalism which allows fitting measured data in the *regime I* is that possibly related to the BKT transition. Nevertheless, so far we do not have direct evidence of it. Therefore, to further evaluate the possible relation between the measured resistance and the BKT transition, in this section we analyse the *I–V* curves taken at different temperatures close to $T'(I)$ and T_{co}. These data will allow also extraction of the critical currents and their temperature dependence.

Figure 5(a) shows the *I–V* curves measured at zero field for a TES with $T_{co} = 467$ mK, at selected temperatures. The double logarithmic scale indicates that the *I–V* curves can be described by a power law with temperature dependent exponents. As argued in the previous section, a power law dependence would be expected for the thermally induced vortex unbinding mechanism, with the exponent *n* changing from well above 3 at temperatures lower than T_{BKT} to $n = 1$ above it. Traditionally, the observation of such a jump has been considered as evidence of the BKT transition.

As shown in figure 5(a), the fits of the measured *I–V* curves to a power law are quite good. Figure 5(b) shows the values of the exponent *n* obtained from these fits for the positive and negative current branches of the *I–V* curves. The fact that the calculated exponents are almost equal for positive and negative currents makes these data very reliable. Contrary to the prediction, there is no abrupt jump in *n* but, instead, it continuously decreases from values much larger

Figure 6. Temperature dependence of the critical currents obtained from the *I–V* curves in figure 5(a). The lines are fits to Ginzburg–Landau power laws, $(1 - T/T_{co})^m$. Inset: dissipation onset for a TES with $T_{co} = 467$ mK, as determined from $R(T)$ and *I–V* data sets.

than 3 at low temperatures, down to values near to 1 for higher temperatures closer to T'_o. However, as already discussed, this abrupt jump is strictly expected to take place in the small current limit and can be smeared out in the presence of finite currents, inhomogeneities or disorder [14, 15, 23–26], which may be our case. Therefore, although these data do not unambiguously proof the existence of a BKT transition, they are compatible with this scenario in the case of a smearing or broadening of the transition.

Figure 6 shows the critical currents $(I_c(T))$ obtained from the *I–V* curves for two TESs with T_{co} of 642 and 467 mK. They cannot be fitted by the exponential law predicted for weak links [2, 27]. This could be expected from the sizes of the devices studied here, since weak link effects usually become evident for TES lengths $L < 50$ μm. Instead, the temperature dependence of the critical currents can be fitted to a Ginzburg–Landau law $(1 - T/T_{co})^m$, with m taking values of 1.6 and 2, respectively. The zero temperature critical currents extracted from these fits are of several tens of mA, about a factor of five to ten above the I_o values extracted from fits to equation (5). This could indicate that the characteristic currents I_o cannot be identified with I_c. It should be noted, however, that the values of the critical currents at zero temperature extrapolated from Ginzburg–Landau laws can be sensibly higher than the actual values of $I_c(T = 0)$, since the Ginzburg–Landau dependences $(1 - T/T_{co})^m$ are valid only in the vicinity of the mean field transition temperature. In fact, all the fundamental parameters of a superconductor, and thus also I_c, are expected to saturate at low temperatures.

The inset in figure 6 shows the resistance onset temperature (T_0) as a function of current and the critical currents extracted from figure 5(a) at different temperatures; the coincidence of the two data sets indicates that both $T_0(I)$ and $I_c(T)$ demark the dissipation onset. Here it must be highlighted the difference between I_c defined as the dissipation onset and the depairing current (I_d) defined as the current capable of breaking the Cooper pairs. In fact, I_c can be much smaller than I_d, when the dissipation is due to other mechanisms such as free vortex motion [6].

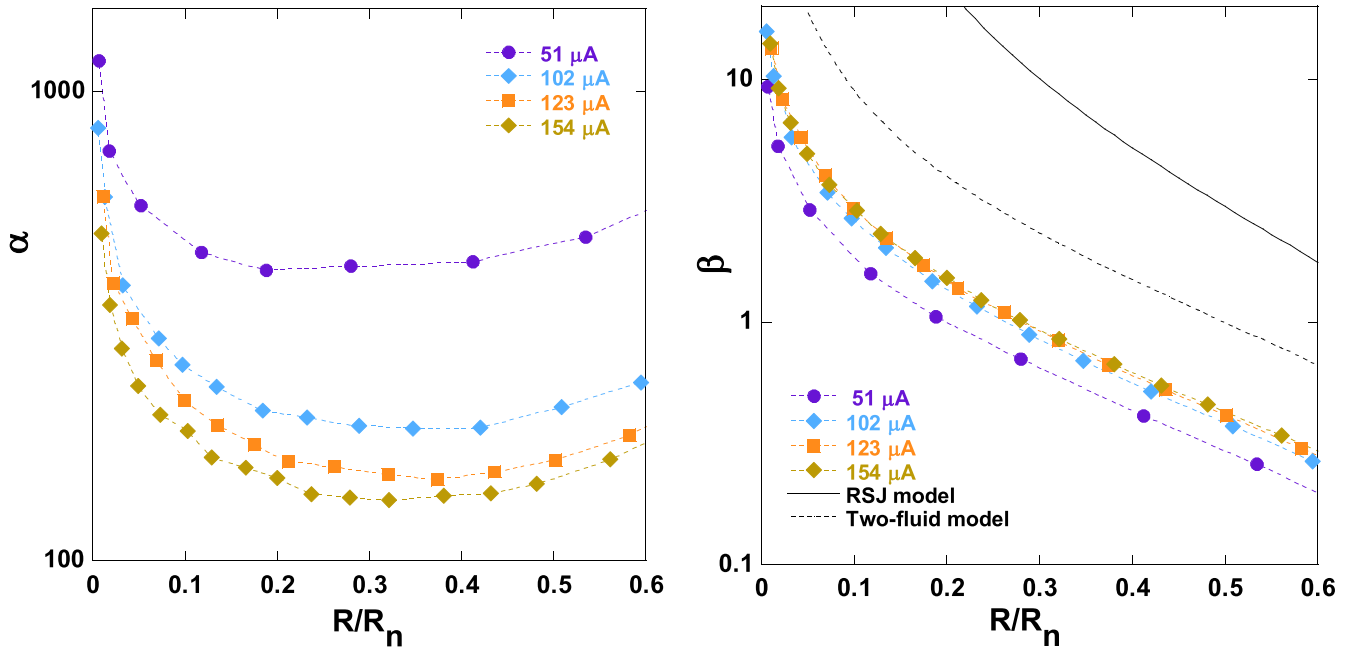### 3.4. Impact of the observed R(T, I) on TESs

In the previous section we have shown the huge broadening of the $R(T)$ transition induced by an external electrical current, and have found an analytical expression to describe the lower part of it at zero external magnetic field. We have argued that the observed $R(T, I)$ behaviour could be ascribed to vortex pair unbinding (BKT transition). In this section we outline some possible implications of the observed $R(T, I)$ behaviour on the TES performances.

The first thing to be mentioned is that the highly nonlinear regime observed for the $R(T)$ curves at $\mu_0 H = 0$ mT in the low resistance region blurs the commonly accepted picture that TESs have a narrow transition with monotonous increase of resistance (single physical mechanism of the whole transition), since according to our data this picture does not hold for the electrical current window typically used for TES biasing. Moreover, the fact that the characteristic temperature of the initial resistance drop remains nearly constant, whereas the onset of dissipation shifts significantly towards lower temperatures with rising current, indicates that care must be taken when defining the critical temperature and the transition width, since the values obtained at low current (from the basic $R(T)$ characterization of the TES transition) may not be suitable for higher currents (biased TES). Also, the validity of the thermal equation $P(T) = K(T^n - T^n_{bath})$, most often used to extract the TES thermal parameters from the *I–V* curves, is questionable, as already shown first by Lindeman *et al* [28] and later by Bailey *et al* [29] when analysing weak link effects. Indeed, the strong dependence of the resistive transition on the external electrical current observed here would have similar consequences to those arising from the weak link dependence. For instance, we note that the thermal conductivity values calculated from the *I–V* data in our 100 mK TES at low R/R_n are in agreement with an underestimate of the thermal conductivity at low R/R_n, which could originate from the non-validity of the approximations used to extract it, when there is a significant transition broadening.

Another important implication of the $R(T, I)$ shape is its effect on the α and β parameters, which describe the sensitivity of the sensor to temperature and current, respectively. On the basis of equations (4) and (5) an expression for α and β can be found by deriving analytically:

$$\alpha \equiv T\frac{\partial LnR}{\partial T}\bigg|_{I=\text{const}} = -\frac{T\,(b')^2}{2\,Ln(R/R_n)}\frac{T_{co} - T'(I)}{(T - T'(I))^2} \quad (6a)$$

$$\beta \equiv I\frac{\partial LnR}{\partial I}\bigg|_{I=\text{const}} = -Ln(R/R_n)\frac{I}{2I_o}\frac{T'_o}{T - T'(I)}. \quad (6b)$$

Figure 7. α (a) and β (b) values calculated from equation (6) using the experimental $R(T, I = \text{const})$ data measured for the TES with $T_{co} = 473$ mK. In (b) the lines corresponding to the values of β predicted in the resistively shunted junction (RSJ) model and in the two-fluid model (respectively equations (16) and (19) in [2]) are shown for comparison.

Equation (6a) is, of course, equivalent to that derived by Fraser [18], but including the current dependence given by equation (5). The α and β values obtained using equation (6) together with the $R(T, I)$ data measured for a TES with $T_{c0} = 473$ mK are shown in figure 7. Here it is observed that α and β strongly depend on the electrical current. α decreases with increasing current. On the contrary β decreases with increasing current, tending to saturate at high currents. Both α and β abruptly decrease with increasing bias, at low R/R_n values; but, while α becomes nearly constant at intermediate R/R_n, β decreases monotonously with increasing R/R_n. These different dependences of α and β should help to optimize the figure of merit of TES.

It is worthwhile to mention that the β values calculated from our data agree with values reported by different groups [2] but are somehow lower than those predicted by the two-fluid model or the long junction limit. It is also remarkable to note that the shape of β as a function of R/R_n is quite similar to that predicted within the two-fluid model [2].

Finally, and most importantly, Fraser [18] evaluated the noise contribution arising from a BKT transition, that is, the phase slip shot noise due to the motion of free vortices when applying an electrical current. According to Fraser, this noise should be white, and vary as $1/R$ and as the reciprocal of the device area; also, it is expected to decrease with increasing the bath temperature, T_{bath}. Preliminary analyses of noise measured in our TESs with $T_{co} \sim 100$ mK reveal an excess noise compatible with these features ($1/R$ dependence and decreasing with increasing T_{bath}). Moreover, the noise values are also in agreement with those expected from [18]. These facts further support the hypothesis that the dissipation measured in the lower part of the resistance transition for the studied TESs relates to the BKT transition, and also to its validity for lower T_c devices.

4. Conclusions

The resistive transition of several TESs has been studied as a function of temperature, external electrical current and external magnetic field. The application of an external electrical current and/or an external magnetic field leads to a broadening of the transition, as a result of the decrease in the temperature delimiting the appearance of a finite resistance.

Focussing on samples measured with an electrical current but without any external magnetic field, we observed two different regimes in the $R(T)$ curves for all devices. Different mechanisms have been studied to account for the experimental observations. Results show that in the lower resistance regime, the behaviour of $R(T, I)$ can be only well fitted using an expression equivalent to that expected for the BKT transition (vortex pair unbinding) but with current dependent characteristic temperatures. A current enhanced vortex pair unbinding mechanism provides a possible interpretation of these results. Nevertheless, when analysing the I–V curves we do not observe the expected jump of the exponent which is considered direct evidence of the BKT transition; this could be probably due to the presence of finite currents, inhomogeneities or disorder. Further studies need to be carried out to unequivocally clarify this point. If confirmed this would be the first indication of a possible BKT in proximity bilayers and in TES devices, to the best of our knowledge.

Finally, we have discussed some possible consequences of the empirical $R(T, I)$ curves on the TESs performances, pointing out the relevance of the biasing current in the

definition of the critical temperature and transition width, questioning the validity of the most often used thermal equation to calculate the thermal parameters for the TES, and describing the strong dependence of α and β on the external current.

The experimental results reported, obtained for TESs with critical temperatures above 400 mK and sizes between 50 and 200 μm, are of interest for the understanding and the optimization of TES operation. Further studies on lower T_c (specially close to 100 mK) and smaller devices should be carried out in order to determine the possible effects of the critical temperature and size on the observed behaviour.

Acknowledgments

ORCID iDs

Lourdes Fàbrega ⓘ https://orcid.org/0000-0002-2611-8037
Agustín Camón ⓘ https://orcid.org/0000-0001-7289-5649
Carlos Pobes ⓘ https://orcid.org/0000-0002-5457-3694

References

[1] Irwin K D and Hilton C C 2005 Transition-edge sensors in cryogenic particle detection *Topics in Applied Physics* ed C Enss vol 99 (Berlin: Springer) pp 63–149
[2] Ullom J N and Bennett D A 2015 *Supercond. Sci. Technol.* **28** 084003
[3] Chiao M P *et al* 2017 *IEEE Trans. Appl. Supercond.* **27** 2100305
[4] Morgan K M, Gard J D, Hays-Wehle J P, Ullom J N, Pappas C G, Bennett D A, Hilton G C, Reintsema C D, Schmidt D R and Swetz D S 2017 *Appl. Phys. Lett.* **110** 21260
[5] Zhang S, Eckart M E, Jaeckel F T, Kripps K L, McCammon D, Morgan K M and Zhou Y 2017 *J. Appl. Phys.* **121** 074503
[6] Blatter G, Feigel'man M V, Geshkenbein V B, Larkin A I and Vinokur V M 1994 *Rev. Mod. Phys.* **66** 1125
[7] Berezinskii V L 1972 *Zh. Eksp. Teor. Fiz.* **61** 1144
Berezinskii V L 1972 *Sov. Phys.—JETP* **34** 610
[8] Kosterlitz J M and Thouless D 1973 *J. Phys. C: Solid State Phys.* **6** 1181
Kosterlitz J M 1974 *J. Phys. C: Solid State Phys.* **7** 1046
[9] Beasley M R, Mooij J E and Orlando T P 1979 *Phys. Rev. Lett.* **42** 1165
[10] Doniach S and Huberman B A 1979 *Phys. Rev. Lett.* **42** 1169
[11] Halperin B I and Nelson D R 1979 *J. Low Temp. Phys.* **36** 599
[12] Hebard A F and Fiory A T 1980 *Phys. Rev. Let.* **44** 291
[13] Hebard A F and Fiory A T 1983 *Phys. Rev. Lett.* **50** 1603
Fiory A T, Hebard A F and Glaberson W I 1983 *Phys. Rev. B* **28** 5075
[14] Hsu J W P and Kapitulnik A 1992 *Phys. Rev. B* **45** 4819
[15] Pierson S W, Friesen M, Ammirata S M, Hunnicutt J C and Gorham L A 1999 *Phys. Rev. B* **60** 1309
[16] Yong J, Lemberger T R, Benfatto L, Ilin K and Siegel M 2013 *Phys. Rev. B* **87** 184505
[17] Baity P G, Shi X, Shi Z, Benfatto L and Popovic D 2016 *Phys. Rev. B* **93** 024519
[18] Fraser G W 2004 *Nucl. Instrum. Methods Phys. Res.* A **523** 234
[19] Galeazzi M 2010 *IEEE Trans. Appl. Supercond.* **21** 267
[20] Fàbrega L, Camón A, Fernández-Martínez I, Sesé J, Parra-Borderías M, Gil O, González-Arrabal R, Costa-Krämer J L and Briones F 2011 *Supercond. Sci. Technol.* **24** 075014
[21] Ezaki S, Maehata K, Iyomoto N, Asano T and Shinozaki B 2018 *J. Appl. Phys.* **123** 084504
[22] Pobes C, Fàbrega L, Camón A, Casañ-Pastor N, Strichovanec P, Sesé J, Moral-Vico J and Jáudenes R 2017 *IEEE Trans. Appl. Supercond.* **27** 2101505
Strichovanec P *et al* Progress on fabrication of Mo/Au based transition-edge sensors through control of edge profiles (in preparation)
[23] Kadin A M, Epstein K and Goldman A M 1983 *Phys. Rev. B* **27** 6691
[24] König E J, Levchenko A, Protopopov I V, Gornyi I V, Burmistrov I S and Mirlin A D 2015 *Phys. Rev. B* **92** 214503
[25] Maccari I, Benfatto L and Castellani C 2017 *Phys. Rev. B* **96** 060508
[26] Sankar S, Vinokur V M and Tripathi V 2018 *Phys. Rev. B* **97** 020507
[27] Sadleir J E, Smith S J, Bandler S R, Chevenak J A and Clem J R 2010 *Phys. Rev. Lett.* **104** 047003
[28] Lindeman M A, Barger K A, Brandl D E, Crowder S G, Rocks L and McCammon D 2008 *J. Low Temp. Phys.* **151** 180
[29] Bailey C N *et al* 2012 *J. Low Temp. Phys.* **167** 121